
Self-supervised Video Object Segmentation

Fangrui Zhu*
Fudan University
xiaoruirui233@gmail.com

Li Zhang*
University of Oxford
lz@robots.ox.uk

Yanwei Fu
Fudan University
yanweifu@fudan.edu.cn

Guodong Guo
West Virginia University
guodong.guo@mail.wvu.edu

Weidi Xie
University of Oxford
weidi@robots.ox.uk

Abstract

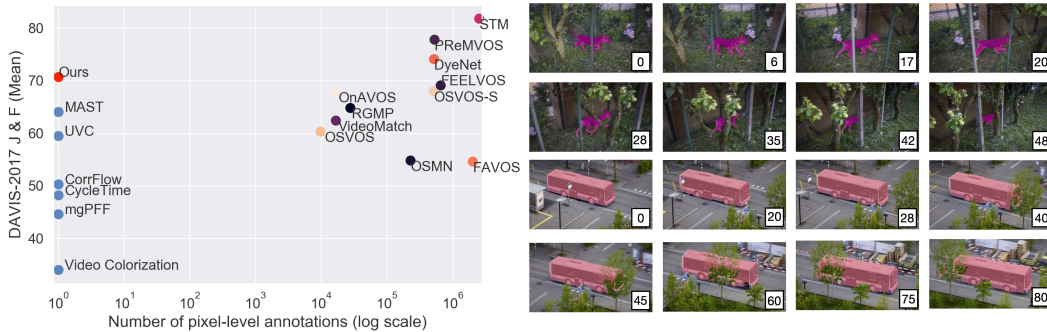
The objective of this paper is self-supervised representation learning, with the goal of solving semi-supervised video object segmentation (*a.k.a.* dense tracking). We make the following contributions: (i) we propose to improve the existing self-supervised approach, with a simple, yet more effective memory mechanism for long-term correspondence matching, which resolves the challenge caused by the disappearance and reappearance of objects; (ii) by augmenting the self-supervised approach with an online adaptation module, our method successfully alleviates tracker drifts caused by spatial-temporal discontinuity, *e.g.* occlusions or dis-occlusions, fast motions; (iii) we explore the efficiency of self-supervised representation learning for dense tracking, surprisingly, we show that a powerful tracking model can be trained with as few as 100 raw video clips (equivalent to a duration of 11mins), indicating that low-level statistics have already been effective for tracking tasks; (iv) we demonstrate state-of-the-art results among the self-supervised approaches on DAVIS-2017 and YouTube-VOS, as well as surpassing most of methods trained with millions of *manual* segmentation annotations, further bridging the gap between self-supervised and supervised learning. Codes are released to foster any further research (https://github.com/fangruizhu/self_sup_semiVOS).

1 Introduction

Reliable and robust tracking is one of the fundamental requirements for intelligent agents, playing a vital role in many computer vision applications, such as vehicle navigation, video surveillance and activity recognition. Generally, the problem is defined as to re-localize the desired object in a video sequence with the best possible accuracy, where the object is identified solely by its location (bounding box) or the pixel-wise segmentation mask in the first frame, referring as visual object tracking (VOT) [1] or semi-supervised video object segmentation (Semi-VOS) [2], respectively. In this paper, we focus on the latter case with possibly multiple objects being present and segmented, and refer to it interchangeably as *dense tracking* from here on.

Several recent studies [3–7] present promising results on self-supervised video object segmentation. Though driven by various motivations, these methods can be thought of as learning pixel-wise correspondences, able to *propagate* the instance segmentation masks along the video sequence. Leveraging the spatio-temporal coherence in natural videos, self-supervised learning is formulated as either minimizing the photometric error between the raw frame and its reconstruction [3, 4, 7] or maximizing the cycle consistency in videos [5, 6]. The outcome of training is an encoder to perform correspondence matching: the feature embedding of pixels in the “query” frame should be close to

*Equal contribution.



(a) Comparison on DAVIS-2017.

(b) Qualitative results.

Figure 1: **Notations:** OnAVOS [11], OSVOS [12], FAVOS [13], CINM [14], VOSwL [15], DyeNet [16], PReMVOS [17], OSVOS-S [18], OSMN [19], RGMP [20], Video Colourization [3], AGAME [21], mgPFF [22], CorrFlow [4], RVOS [23], FEELVOS [24], SiamMask [25], CycleTime [5], RANet [26], UVC [6], MAST [7].

their matching pixels in “reference” frames and far away from other unrelated pixels. Despite being simple, these self-supervised approaches are still challenged by the existence of spatio-temporal discontinuities, *e.g.* occlusions, fast motion, motion blur, and textureless surfaces, which eventually lead accumulated errors and tracker drifts.

From this perspective, we hypothesize that it is desirable to augment the existing self-supervised approaches with *online adaptations* – maintain an appearance model for the object of interest in each video sequence [8], continuously updating the propagated masks during inference time, *e.g.* cleaning up error drifts. To be clear, this is fundamentally different from the common paradigms that adapt representations acquired from large-scale supervised learning. Here, in our case, the appearance model is always *randomly initialised* for each video sequence, parameters of which are only trained on the imperfect masks obtained from propagation. Thus it still falls into the self-supervised paradigm.

A general concern for the self-supervised online adaptation is that it could potentially overfit to the imperfect masks, ending up with exactly the same predictions as those from mask propagations. After all, deep networks have shown the capability of even overfitting to random labels [9]. However, our key insight is that the model tends to learn the regularities in data faster than stochastic noises, a phenomenon originally discovered in [10]. This property is especially suitable in our self-supervised online adaptation, as the appearance model is complementary to mask propagation, *i.e.* less dependent on temporal coherence, making it less likely to make the same mistakes as propagation-based models do. We will return to this point in Section 3.3.

In addition, we also show that, contrary to the belief that dense tracking requires good *semantic* representation, we train a powerful model with as few as 100 raw videos (with a duration of around 10mins) or even 100 still images through self-supervised learning, being able to surpass a number of approaches that are trained with in a fully supervised manner. This is particularly remarkable, as it may indicate **supervised learning or semantic representation is not of the essence for dense tracking (semi-VOS)**, helping to form a solid belief on self-supervised approaches.

To this end, we summarize our contribution as following: (i) we revisit the state-of-the-art self-supervised approach (MAST [7]) for dense tracking (semi-VOS), and propose a simple, yet more effective memory mechanism to enable long-term correspondences, *i.e.* matching beyond pairwise frames to resolve the challenge caused by disappearance and reappearance of objects; (ii) propose a novel *self-supervised online adaptation* that complements the existing propagation-based approach, and show it is beneficial for alleviating tracker drifts; (iii) conduct a pilot study to show the surprisingly high efficiency for self-supervised representation learning. (iv) demonstrate state-of-the-art results among self-supervised approaches on standard benchmarks, *e.g.* DAVIS-2017 and YouTube-VOS, surpassing the majority of methods trained with millions of manual annotations, further bridging the gap between self-supervised and supervised learning.

2 Related work

Self-supervised representation learning has recently shown to be an promising alternative to supervised learning on a variety of downstream tasks [27–30]. In the literature, numerous pretext

tasks have been proposed for learning semantics from free supervision signals residing in images and videos. These include creating pseudo classification labels [31], exploring spatial context in images [32] and temporal ordering in videos [33], such as predicting jigsaw puzzles [34], shuffled frames [35], motion [36], the arrow of time [37], predicting future representations [38, 39].

Semi-supervised video object segmentation (Semi-VOS) aims to re-localize one or multiple targets that have been specified in the first frame of a video with pixel-wise segmentation masks. Prior works can be roughly divided into two categories, one is based on mask propagation [40, 24, 25], and the other is related with few shot learning or online adaptations [41, 11, 12]. Commonly, extensive human annotations are required to train such systems. More specifically, they generally adopt a deep neural network with its backbone network (*e.g.* ResNet) pretrained on ImageNet [42] and finetune the whole framework on COCO [43], DAVIS [2] and Youtube-VOS [44], *etc.* Alternatively, recent approaches [3, 5–7] based on self-supervised learning have shown great potentials.

Learning with imperfect segmentation has been studied for aerial images [45, 46] in the literature. Here, we share the same spirit that the proposed self-supervised online adaptation module can only be trained on imperfect masks generated from propagation through correspondence matching.

3 Method

In this section, we first review the previous self-supervised approaches for dense tracking, specifically, the ones target on learning pixel-wise correspondences through frame reconstruction (Section 3.1). Next, in Section 3.2, we propose a simple, momentum memory mechanism that enables long-term correspondence matching, yet without incurring the bottleneck from the physical hardware memories. Finally, in Section 3.3, we describe the proposed self-supervised online adaptation module.

3.1 Learning correspondence through reconstruction

In the recent work [3, 4, 7], learning pixel-wise correspondence in videos has been formulated as the outcome of frame reconstruction. Specifically, with the use of certain information bottleneck, each pixel from the ‘query’ frame is forced to find pixels that can best reconstruct itself in one or multiple ‘reference’ frames.

Mathematically, given a pair of frames from a video clip, *e.g.* $\{I_{t-1}, I_t\} \in \mathcal{R}^{H \times W \times 3}$, we parameterise the feature encoder with a ConvNet ($\Phi(\cdot; \theta)$), *i.e.* $f_t = \Phi(g(I_t); \theta)$, where $f_t \in \mathcal{R}^{h \times w \times d}$ (height, width and channels respectively), $g(\cdot)$ denotes a bottleneck that prevents information leakage. For instance, in [3], it refers to the RGB2Gray operation; in [7], a simple channel-wise dropout in Lab colour space has shown to be surprisingly powerful.

To this end, an affinity matrix (A) is computed as a soft attention, denoting the strength of the similarity between pixels in ‘query’ frame (I_t) and those in the ‘reference’ frame (I_{t-1}). Leveraging the spatio-temporal coherence in videos, a pixel i in I_t can be represented as a weighted sum of pixels in I_{t-1} . To avoid abuse of notations, spatial positions in the frame are represented with a single character (*e.g.* i, j). Normally, we only consider pixels within a spatial neighbourhood to i , *i.e.* $\mathcal{N} = \{\forall n \in I_{t-1}, |n - i| < c\}$:

$$\hat{I}_t^i = \sum_{j \in \mathcal{N}} A_t^{ij} I_{t-1}^j \quad (1)$$

$$A_t^{ij} = \frac{\exp \langle f_t^i, f_{t-1}^j \rangle}{\sum_{n \in \mathcal{N}} \exp \langle f_t^i, f_{t-1}^n \rangle} \quad (2)$$

where c refers to the radius of neighborhood, and $A_t \in \mathcal{R}^{hw \times 4c^2}$. The outcome of training is an encoder ($\Phi(\cdot; \theta)$) to perform correspondence matching by minimizing some photometric loss (*e.g.* Huber loss), *i.e.* the feature embedding of pixels in the “query” frame should be close to their matching pixels in “reference” frames and far away from other unrelated pixels.

$$\hat{\theta} = \underset{\theta}{\operatorname{argmin}} \mathcal{L}(I_t, \hat{I}_t) \quad (3)$$

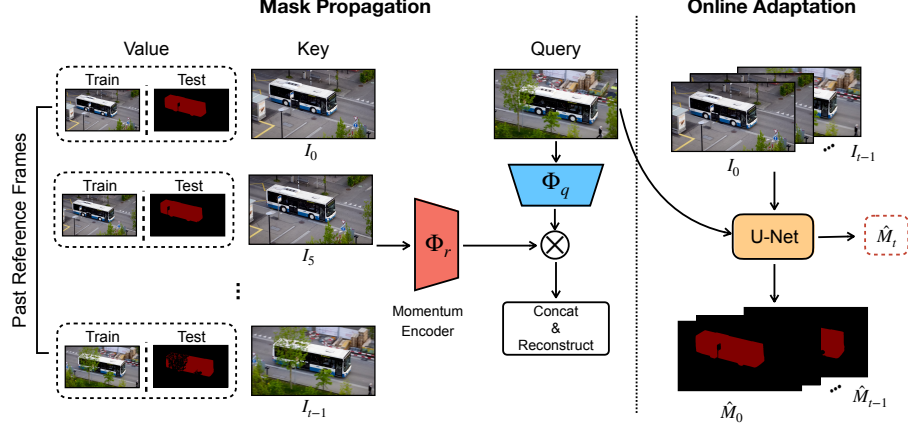


Figure 2: Schematic illustration of the proposed method, *i.e.* self-supervised representation learning and mask propagation, and online adaptation during inference time.

During inference, the same affinity matrix is computed to *propagate* the instance segmentation mask:

$$\hat{y}_t^i = \sum_{j \in \mathcal{N}} A_t^{ij} y_{t-1}^j \quad (4)$$

y_t refers to the segmentation mask for the t -th frame.

3.2 Occlusion-aware mask propagation

One issue with learning correspondence from pairwise frames is that, it can not effectively deal with object disappearance and reappearance. For example, if the object is occluded in one frame (I_t), and re-appear in the next one (I_{t+1}), pairwise matching is deemed to fail as the object in I_{t+1} cannot find its counter part in previous frame (I_t). In psychology, this refers to a fundamental concept – object permanence, the capability of understanding that objects continue to exist even when they cannot be seen, heard, touched, smelled or sensed.

Computationally, a straightforward idea is to maintain an external memory, caching multiple frames for potential correspondence matching. In this paper, we propose a momentum memory, which significantly simplify the memory training in [7], able to cache as long as the entire video sequence, without incurring the bottleneck from the limitation of physical GPU memory.

Formally, given a query frame I_q and an external memory bank with K frames, *e.g.* $I_r = \{I_1, \dots, I_K\} \in \mathcal{R}^{K \times H \times W \times 3}$, we parameterize two ConvNets, *e.g.* $\Phi_q(\cdot; \theta_q)$ and $\Phi_r(\cdot; \theta_r)$, to compute representations for query and reference frames:

$$f_q, f_r = \Phi_q(I_q; \theta_q), \Phi_r(I_r; \theta_r) \quad (5)$$

The reconstruction of the query frame I_q in pixel i becomes:

$$\hat{I}_q^i = \sum_{j \in \mathcal{N}} A_q^{ij} I_r^j \quad (6)$$

$$A_q^{ij} = \frac{\exp \langle f_q^i, f_r^j \rangle}{\sum_{n \in \mathcal{N}} \exp \langle f_q^i, f_r^n \rangle} \quad (7)$$

where $A_q \in \mathcal{R}^{hw \times K4c^2}$, $\mathcal{N} = \{\forall n \in I_r, |n - i| < c\}$. In practice, the number of reference frame can be varied, we use 5 (with the first frame always included) as it provides a balance between performance and computation (shown in Section 4.3).

While training, θ_q is updated with standard back-propagation, and θ_r is updated with momentum, similar to [29]:

$$\theta_r \leftarrow m\theta_r + (1 - m)\theta_q \quad (8)$$

Here $m \in [0, 1)$ is a momentum coefficient. In our case, we use $m = 0.999$ in the experiments (ablation studies have been shown in Section 4.3). To this end, we can train a complete model, the feature encoder ($\Phi_q(\cdot; \theta_q), \Phi_r(\cdot; \theta_r)$) by self-supervised frame reconstruction, and use it to *propagate* the mask from initial frame to subsequent ones in the video sequence.

3.3 Self-supervised online adaptation

Despite being effective for understanding object permanence, the memory mechanism still suffers from spatio-temporal discontinuity, *e.g.* occlusion or disocclusions (regions that are originally occluded in all previous frames become visible). Under these scenarios, self-supervised approaches based on low-level statistics (photometric consistency in frame reconstruction) become insufficient to establish reliable correspondences, eventually leading to accumulated errors and tracker drifts. As an extension to the propagation-based tracker, we propose to incorporate an online adaptation module to fit the appearance of the target instances [8].

Specifically, during the inference stage, for frame I_t in a test video sequence, we can easily obtain the mask predictions for all previous frames from correspondence propagation (Eq 4), denoted as $\{(I_1, y_1), (I_2, \hat{y}_2), \dots, (I_t, \hat{y}_t)\}$, where the y_i, \hat{y}_i refer to the ground-truth segmentation mask and prediction from correspondence matching (mask propagation) respectively. Note that, the ground-truth segmentation mask is only available for the first frame in the video sequence.

With these segmentation masks, we are able to train an appearance model (*e.g.* frame-wise segmentation model, $\Psi(\cdot; \theta_o)$) from *scratch* for each video sequence, where:

$$\hat{\theta}_o = \operatorname{argmin}_{\theta_o} \mathbb{E} [\mathcal{L}(\Psi(I_i; \theta_o), \hat{y}_i)] \quad (9)$$

In practice, we adopt a simple U-Net [47] as the appearance model (details in Section 4.1). Note that, this is fundamentally different from the the previous online adaptation approaches [11], as we do not require any supervised pre-training or complex sample minings. In fact, for each video sequence, there is always one tailored appearance network training from *scratch*.

Discussion. A general concern for such self-supervised online adaptation is that it could potentially overfit to the imperfect masks, ending up with same predictions as the mask propagation. However, in practice, as the online adaptation module is complementary to the propagation-based approach, we observe it is indeed possible to train a deep network on single video sequence with imperfect masks. To be specific, propagation can usually solve smooth object deformations with its built-in spatio-temporal coherence, but fails when faced with discontinuity (regions that have been invisible till this time point). In contrast, the appearance model treats each frame independently, as the same object instances in a video sequence often show far higher similarity (self-similarity) than with the background, the built-in prior in ConvNets therefore tends to grasp the regularities in data before overfitting to noises, a phenomenon originally observed in [10]. We experimentally show this phenomenon in Section 4.2.

4 Experiments

In this section, we first introduce the datasets and implementation details in Section 4.1, and then describe the training process for learning dense correspondence and the online adaptation in Section 4.2. We further examine the effects of different components in Section 4.3. With the optimal settings, we conduct a pilot study with the goal of better understanding the essence of tracking (Section 4.4), specifically, on the role of semantic supervision. Lastly, we show comparison to the state-of-the-art Semi-VOS approaches in Section 4.5.

4.1 Experimental setup

Datasets and evaluation. We conduct experiments on two widely-used datasets, DAVIS-2017 [2] and YouTube-VOS [44]. Specifically, DAVIS-2017 contains 150 HD videos with over 30K instance segmentation annotations, and YouTube-VOS has over 4,000 HD videos of 90 semantic categories with over 190K instance segmentation annotations. In this paper, all training has been done on the YouTube-VOS training set in a self-supervised manner, *i.e.* *zero* groundtruth segmentation annotation is used during training time.

For evaluation, we benchmark on the official semi-supervised video object segmentation protocol of DAVIS-2017, and YouTube-VOS 2018 val set, that is, ground-truth segmentation mask is only given in the first frame, and the goal is to predict the object mask in subsequent frames. Standard evaluation metrics are used, namely, region similarity (\mathcal{J}) and contour accuracy (\mathcal{F}).

Implementation details. For learning correspondence, we adopt a ResNet-18 as our feature encoder, same as in [7], it produces feature embeddings with spatial resolution of $1/4$ of the original image. As pre-processing, we randomly crop the original images and resize them to the size of 384×384 . The same data augmentation is applied as in [7], *e.g.* *Lab* space inputs for both the query and reference frames with random colour jittering ($p = 0.3$) and channel dropout ($p = 0.5$).

In detail, we first pretrain the feature encoder with pairwise inputs for 120K iterations and batch size of 48 with Adam optimiser. After pretraining, we finetune the model with a momentum memory, where multiple previous frames are treated as references, and a smaller learning rate of 1×10^{-4} is applied for another 10K iterations. The window size for neighbourhood is set to 25pix in our training.

During inference time, the affinity matrix is computed between the query and reference frames in the memory, and further used for propagating the desired pixel-level segmentation masks. At the same time, we start the online adaptation procedure, *i.e.* train an appearance model on each video sequence with the frames in memory as inputs and their predicted instance masks as the pseudo ground-truth. For simplicity, the appearance model uses a U-Net [47] with ResNet-18 backbone. All inputs are resized to 480×480 with random colour jittering, gray-scaling and horizontal flipping. Note that, we train the appearance model *from scratch* for each test sequence, without updating the feature encoder ($\Phi(\cdot)$). Adam optimiser is used, with an initial learning rate of 2×10^{-4} , decaying with the step size of 50. The entire adaptation process lasts for around 200 iterations, and the outputs from appearance model are treated as final predictions.

4.2 Self-supervised online adaptation

In this section, we aim to validate the idea of training an appearance model from imperfect segmentation masks. Specifically, we assume there exists an *oracle* with the access to ground-truth, such that the learning process for online adaptation can be monitored. In Figure 3, we compare the prediction from online adaptation (appearance model) with mask propagation (Figure 3a), and with ground-truth masks provided by the *oracle* (Figure 3b), dash lines can be seen as the baseline, indicating the raw performance of mask propagation. Note that, manual segmentation masks are only used to plot this curve, but *never* be used for training the appearance model.

As can be seen in Figure 3b, the appearance model quickly absorbs information from the propagated segmentation masks, outperforming the baselines (shown by dash lines) from mask propagation. However, with more training iterations, the model starts to give inferior predictions. This phenomenon confirms our conjecture that the structure of ConvNets has enforced a strong prior on image statistics [10], which enables the model to grasp the regularities (self-similarity of the instances) in data before overfitting to error drifts. Another phenomenon is, the best appearance models can always be obtained at the stage, where the learning process starts to get slow, roughly around 150-250 iterations. In the following online adaptation experiments, we thus decide to train only 200 iterations.

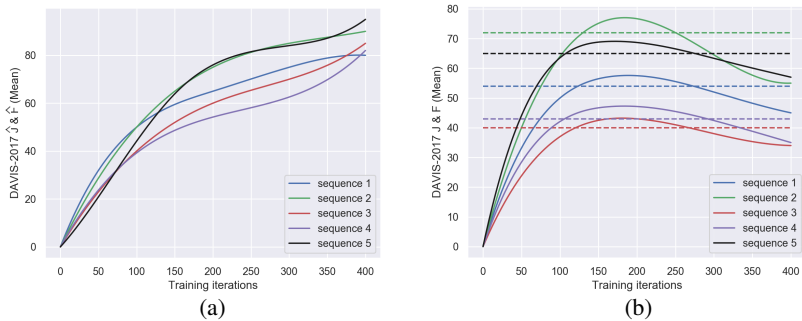


Figure 3: Learning process of the self-supervised online adaptation module. In (a), $\hat{\mathcal{J}} \& \hat{\mathcal{F}}$ (mean) is computed between the predictions from appearance model and the propagated masks (pseudo groundtruth). In (b), $\mathcal{J} \& \mathcal{F}$ (mean) is computed between the predictions from appearance model and manual ground-truth masks acquired from an *oracle*. Dash lines denote the baseline between propagated masks and groundtruth.

4.3 Ablation studies

To examine the effectiveness of different components, we conduct a series of experiments by adding one component at a time, *e.g.* momentum memory, online adaptation. All models are trained on YouTube-VOS, and evaluated on DAVIS-2017 semi-supervised video object segmentation protocol.

Variants	DAVIS-2017		
	$\mathcal{J}\&\mathcal{F}$	$\mathcal{J}(\text{Mean})$	$\mathcal{F}(\text{Mean})$
MAST pairwise [7]	59.6	57.3	61.8
+ memory (MAST [7])	63.8	61.2	66.3
Ours (pairwise)	60.4	58.7	62.0
+ momentum memory	68.2	66.5	69.9
+ online adaptation	70.7	68.2	73.1

Table 1: Effects of the proposed modules, *e.g.* momentum memory, online adaptations.

variants	number	DAVIS-2017		
		$\mathcal{J}\&\mathcal{F}$	$\mathcal{J}(\text{Mean})$	$\mathcal{F}(\text{Mean})$
# ref frames	1	60.4	58.7	62.0
	3	65.0	63.6	66.2
	5	68.2	66.5	69.9
	t-1	66.4	65.0	67.8

Table 2: Effects of the number of reference frames in memory while propagating masks to t -th frame. $t-1$ refers to the extreme case of caching all previous frames.

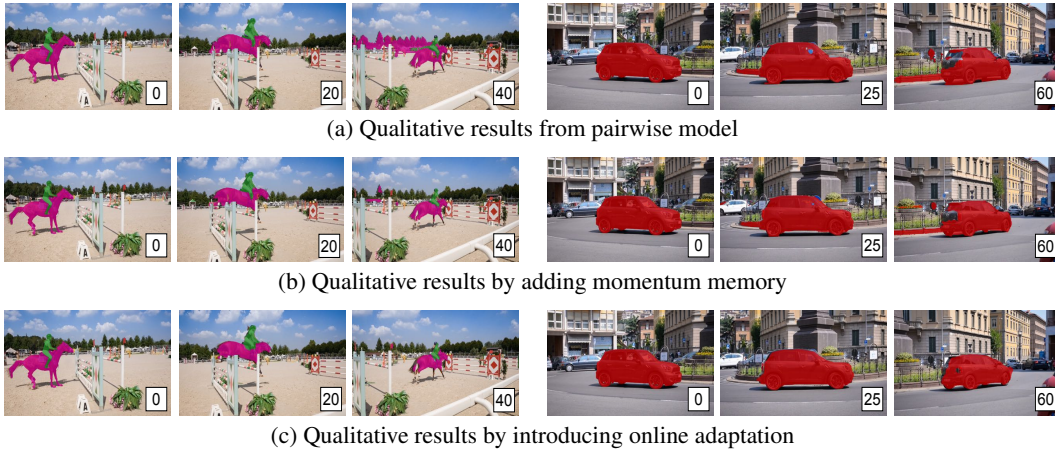


Figure 4: Qualitative comparison for the effectiveness of the proposed modules.

We first re-implement the pairwise model from MAST [7] (59.6 vs 60.4). As shown in Table 1, the proposed momentum memory brings a significant performance boost, from 60.4 to 68.2 on $\mathcal{J}\&\mathcal{F}$. In addition, the proposed self-supervised online adaptation module further improves on the high baseline (from 68.2 to 70.7 on $\mathcal{J}\&\mathcal{F}$).

Next, we study the effect of using different number of reference frames in the memory bank. As shown in Table 2, it is clear that the memory module (with more than one reference frame) plays a vital role for this task, but the model is fairly robust to the number of reference frames. Thus, we choose to use 5 reference frames in the following experiment, as it gives the optimal performance, yet still be efficient during inference time.

In Figure 4, we show the qualitative comparisons by adding one components at a time. The model based on pairwise frame propagation suffers serious error drifts, *e.g.* horse masks drift to the background, the car masks drift to the road. For both cases, the errors are caused by the dis-occlusion, *i.e.* the regions that are originally hidden start to show up. With the help of momentum memory and online adaptation, errors have been significantly alleviated.

4.4 Data efficiency for self-supervised training

In this section, we conduct a study for learning powerful representations under a low-data regime. Specifically, we consider experiments in two settings, namely, only training a small number of images or real videos. For images, we use simple homography transformations to augment images into video sequences, and the proposed model is then trained on these simulated sequences. In comparison, we also train the same model with only 100 raw videos (a duration of around 10mins).

As shown in Table 3, despite only a small number of images or videos are used for training, the model still performs remarkably well, *i.e.* matching the previous

Training	Variants	DAVIS-2017	
		$\mathcal{J}(\text{Mean})$	$\mathcal{F}(\text{Mean})$
100 videos	pairwise	54.7	57.8
	+ memory	62.5	65.5
	+ adaptation	64.0	66.7
100 images	pairwise	53.7	56.2
	+ memory	60.0	63.1
	+ adaptation	62.1	64.5

Table 3: Efficient self-supervised learning, evaluated on DAVIS-2017 validation sets.

state-of-the-art self-supervised learning approach [7], and outperforming many supervised methods in Table 4. It implies that supervised learning or semantic representation may be not essential in dense tracking, since there is merely any semantic information under such a low-data training regime.

4.5 Compare with state-of-the-art

In this section, we compare with state-of-the-art approaches on DAVIS-2017 (Table 4) and YouTube-VOS (Table 5) semi-VOS benchmarks. Note that, there has been a rapid progress in this research line, here, we only try to compare with the recent state-of-the-art approaches. As different architectures and training set were used in the previous work, which makes fair comparison extremely difficult.

Method	Date	Arch.	Sup.	Dataset	$\mathcal{J}\&\mathcal{F}$	$\mathcal{J}(\text{Mean})$	$\mathcal{J}(\text{Recall})$	$\mathcal{F}(\text{Mean})$	$\mathcal{F}(\text{Recall})$
Vid. Color. [3]	2018	ResNet-18	✗	K(800 hrs)	34.0	34.6	34.1	32.7	26.8
CycleTime [5]	2019	ResNet-50	✗	V(344 hrs)	48.7	46.4	50.0	50.0	48.0
CorrFlow [4]	2019	ResNet-18	✗	O(14 hrs)	50.3	48.4	53.2	52.2	56.0
UVC [6]	2019	ResNet-18	✗	K(800 hrs)	59.5	57.7	68.3	61.3	69.8
MAST [7]	2020	ResNet-18	✗	Y(5.58 hrs)	65.5	63.3	73.2	67.6	77.7
Ours	2020	ResNet-18	✗	DY*(11 mins)	65.4	64.0	71.6	66.7	75.8
Ours	2020	ResNet-18	✗	Y(5.58 hrs)	70.7	68.2	77.8	73.1	83.5
ImageNet [48]	2016	ResNet-50	✓	I	49.7	50.3	-	49.0	-
OSVOS [12]	2017	VGG-16	✓	ID	60.3	56.6	63.8	63.9	73.8
OnAVOS [11]	2017	ResNet-38	✓	ICPD	65.4	61.6	67.4	69.1	75.4
OSMN [49]	2018	VGG-16	✓	ICD	54.8	52.5	60.9	57.1	66.1
OSVOS-S [41]	2018	VGG-16	✓	IPD	68.0	64.7	74.2	71.3	80.7
PRemVOS [17]	2018	ResNet-101	✓	ICDPM	77.8	73.9	83.1	81.8	88.9
SiamMask [25]	2019	ResNet-50	✓	ICY	56.4	54.3	62.8	58.5	67.5
FEELVOS [24]	2019	Xception-65	✓	ICDY	71.5	69.1	79.1	74.0	83.8
STM [40]	2019	ResNet-50	✓	IDY	81.8	79.2	-	84.3	-

Table 4: Quantitative results of multi-object video object segmentation on DAVIS-2017 validation set. Dataset notations: I=ImageNet, C=COCO, D=DAVIS, P=PASCAL-VOC, Y=YouTube-VOS, DY*=randomly sample 100 videos from DAVIS and YouTube-VOS, both from training sets only, K=Kinetics, V=VLOG, O=OxUvA. Results of other methods are directly copied from [7, 40].

As shown by the results from DAVIS-2017 and YouTube-VOS benchmarks, we can draw the following conclusions: *First*, our proposed model clearly outperforms all other self-supervised methods, surpassing previous state-of-the-art [7] by a significant margin (as measured by $\mathcal{J}\&\mathcal{F}$, 65.5 vs 70.7 on DAVIS-2017, 64.2 vs 67.3 on YouTube-VOS). *Second*, compared with the supervised approaches that have been heavily trained with expensive segmentation annotations, our proposed model trained with self-supervised learning can actually outperform the majority of them. *Third*, our proposed approach is shown to be category-agnostic, and can generalize to unseen categories with *no* performance drop, as shown by testing on unseen categories (Table 5).

5 Conclusion

To summarise, in this paper, we have demonstrated the possibility of training competitive models for video object segmentation (dense tracking) without using *any* manual annotations. To achieve that, we introduced a simple, yet effective memory mechanism for long-term correspondence learning, and the online adaptation during inference time. In addition, we show that, contrary to the belief that dense tracking requires good *semantic* representation, competitive models can be trained with as few as 100 raw videos, indicating that supervised learning may not be essential for such a task. We hope our discovery will shed light on potential research of this direction.

Method	Sup.	Overall	Seen		Unseen	
			\mathcal{J}	\mathcal{F}	\mathcal{J}	\mathcal{F}
Vid. Color. [3]	✗	38.9	43.1	38.6	36.6	37.4
CorrFlow [4]	✗	46.6	50.6	46.6	43.8	45.6
MAST [7]	✗	64.2	63.9	64.9	60.3	67.7
Ours	✗	67.3	67.2	67.9	63.2	70.6
OSMN [49]	✓	51.2	60.0	60.1	40.6	44.0
MSK [50]	✓	53.1	59.9	59.5	45.0	47.9
RGMP [51]	✓	53.8	59.5	-	45.2	-
OnAVOS [11]	✓	55.2	60.1	62.7	46.6	51.4
S2S [44]	✓	64.4	71.0	70.0	55.5	61.2
A-GAME [52]	✓	66.1	67.8	-	60.8	-
STM [40]	✓	79.4	79.7	84.2	72.8	80.9

Table 5: Quantitative results on Youtube-VOS validation set. The proposed approach outperforms all previous self-supervised ones, and compare favorably with the models trained with large-scale supervised learning.

References

- [1] Matej Kristan, Jiri Matas, Aleš Leonardis, Tomáš Vojř, Roman Pflugfelder, Gustavo Fernandez, Georg Nebehay, Fatih Porikli, and Luka Čehovin. A novel performance evaluation methodology for single-target trackers. *TPAMI*, 2016.
- [2] Jordi Pont-Tuset, Federico Perazzi, Sergi Caelles, Pablo Arbeláez, Alex Sorkine-Hornung, and Luc Van Gool. The 2017 davis challenge on video object segmentation. *arXiv*, 2017.
- [3] Carl Vondrick, Abhinav Shrivastava, Alireza Fathi, Sergio Guadarrama, and Kevin Murphy. Tracking emerges by coloring videos. In *ECCV*, 2018.
- [4] Zihang Lai and Weidi Xie. Self-supervised learning for video correspondence flow. In *BMVC*, 2019.
- [5] Xiaolong Wang, Allan Jabri, and Alexei A Efros. Learning correspondence from the cycle-consistency of time. In *CVPR*, 2019.
- [6] Xueting Li, Sifei Liu, Shalini De Mello, Xiaolong Wang, Jan Kautz, and Ming-Hsuan Yang. Joint-task self-supervised learning for temporal correspondence. In *NeurIPS*, 2019.
- [7] Zihang Lai, Erika Lu, and Weidi Xie. Mast: A memory-augmented self-supervised tracker. In *CVPR*, 2020.
- [8] Deva Ramanan, David A. Forsyth, and Andrew Zisserman. Tracking people by learning their appearance. *TPAMI*, 2007.
- [9] Chiyuan Zhang, Samy Bengio, Moritz Hardt, Benjamin Recht, and Oriol Vinyals. Understanding deep learning requires rethinking generalization. In *ICLR*, 2017.
- [10] Dmitry Ulyanov, Andrea Vedaldi, and Victor Lempitsky. Deep image prior. In *CVPR*, 2018.
- [11] Paul Voigtlaender and Bastian Leibe. Online adaptation of convolutional neural networks for video object segmentation. *arXiv*, 2017.
- [12] Sergi Caelles, Kevis-Kokitsi Maninis, Jordi Pont-Tuset, Laura Leal-Taixé, Daniel Cremers, and Luc Van Gool. One-shot video object segmentation. In *CVPR*, 2017.
- [13] Jingchun Cheng, Yi-Hsuan Tsai, Wei-Chih Hung, Shengjin Wang, and Ming-Hsuan Yang. Fast and accurate online video object segmentation via tracking parts. In *CVPR*, 2018.
- [14] Linchao Bao, Baoyuan Wu, and Wei Liu. Cnn in mrf: Video object segmentation via inference in a cnn-based higher-order spatio-temporal mrf. In *CVPR*, 2018.
- [15] A. Khoreva, A. Rohrbach, and B. Schiele. Video object segmentation with language referring expressions. In *ACCV*, 2018.
- [16] Xiaoxiao Li and Chen Change Loy. Video object segmentation with joint re-identification and attention-aware mask propagation. In *ECCV*, 2018.
- [17] Jonathon Luiten, Paul Voigtlaender, and Bastian Leibe. Premvos: Proposal-generation, refinement and merging for video object segmentation. In *ACCV*, 2018.
- [18] Kevis-Kokitsi Maninis, Sergi Caelles, Yuhua Chen, Jordi Pont-Tuset, Laura Leal-Taixé, Daniel Cremers, and Luc Van Gool. Video object segmentation without temporal information. *TPAMI*, 2018.
- [19] Linjie Yang, Yanran Wang, Xuehan Xiong, Jianchao Yang, and Aggelos Katsaggelos. Efficient video object segmentation via network modulation. In *CVPR*, 2018.
- [20] Seoung Wug Oh, Joon-Young Lee, Kalyan Sunkavalli, and Seon Joo Kim. Fast video object segmentation by reference-guided mask propagation. In *CVPR*, 2018.
- [21] Joakim Johnander, Martin Danelljan, Emil Brissman, Fahad Shahbaz Khan, and Michael Felsberg. A generative appearance model for end-to-end video object segmentation. In *CVPR*, 2019.
- [22] Shu Kong and Charless Fowlkes. Multigrid predictive filter flow for unsupervised learning on videos. *arXiv*, 2019.
- [23] Carles Ventura, Miriam Bellver, Andreu Girbau, Amaia Salvador, Ferran Marques, and Xavier Giro-i Nieto. Rvos: End-to-end recurrent network for video object segmentation. In *CVPR*, 2019.

- [24] Paul Voigtlaender, Yuning Chai, Florian Schroff, Hartwig Adam, Bastian Leibe, and Liang-Chieh Chen. Feelvos: Fast end-to-end embedding learning for video object segmentation. In *CVPR*, 2019.
- [25] Qiang Wang, Li Zhang, Luca Bertinetto, Weiming Hu, and Philip HS Torr. Fast online object tracking and segmentation: A unifying approach. In *CVPR*, 2019.
- [26] Ziqin Wang, Jun Xu, Li Liu, Fan Zhu, and Ling Shao. Ranet: Ranking attention network for fast video object segmentation. In *ICCV*, 2019.
- [27] Aäron van den Oord, Yazhe Li, and Oriol Vinyals. Representation learning with contrastive predictive coding. *arXiv*, 2018.
- [28] Olivier J. Hénaff, Ali Razavi, Carl Doersch, S. M. Ali Eslami, and Aäron van den Oord. Data-efficient image recognition with contrastive predictive coding. *arXiv*, 2019.
- [29] Kaiming He, Haoqi Fan, Yuxin Wu, Saining Xie, and Ross Girshick. Momentum contrast for unsupervised visual representation learning. In *CVPR*, 2020.
- [30] Ting Chen, Simon Kornblith, Mohammad Norouzi, and Geoffrey Hinton. A simple framework for contrastive learning of visual representations. *arXiv*, 2020.
- [31] Spyros Gidaris, Praveer Singh, and Nikos Komodakis. Unsupervised representation learning by predicting image rotations. *arXiv*, 2018.
- [32] Carl Doersch, Abhinav Gupta, and Alexei A Efros. Unsupervised visual representation learning by context prediction. In *ICCV*, 2015.
- [33] Mehdi Noroozi and Paolo Favaro. Unsupervised learning of visual representations by solving jigsaw puzzles. In *ECCV*, 2016.
- [34] Dahun Kim, Donghyeon Cho, and In So Kweon. Self-supervised video representation learning with space-time cubic puzzles. In *AAAI*, 2019.
- [35] Ishan Misra, C Lawrence Zitnick, and Martial Hebert. Shuffle and learn: unsupervised learning using temporal order verification. In *ECCV*, 2016.
- [36] Jiangliu Wang, Jianbo Jiao, Linchao Bao, Shengfeng He, Yunhui Liu, and Wei Liu. Self-supervised spatio-temporal representation learning for videos by predicting motion and appearance statistics. In *CVPR*, 2019.
- [37] Donglai Wei, Joseph J Lim, Andrew Zisserman, and William T Freeman. Learning and using the arrow of time. In *CVPR*, 2018.
- [38] Carl Vondrick, Hamed Pirsiavash, and Antonio Torralba. Anticipating visual representations from unlabelled video. In *CVPR*, 2016.
- [39] Tengda Han, Weidi Xie, and Andrew Zisserman. Video representation learning by dense predictive coding. In *ICCV*, 2019.
- [40] Seoung Wug Oh, Joon-Young Lee, Ning Xu, and Seon Joo Kim. Video object segmentation using space-time memory networks. In *ICCV*, 2019.
- [41] K-K Maninis, Sergi Caelles, Yuhua Chen, Jordi Pont-Tuset, Laura Leal-Taixé, Daniel Cremers, and Luc Van Gool. Video object segmentation without temporal information. *TPAMI*, 2018.
- [42] Olga Russakovsky, Jia Deng, Hao Su, Jonathan Krause, Sanjeev Satheesh, Sean Ma, Zhiheng Huang, Andrej Karpathy, Aditya Khosla, Michael Bernstein, et al. Imagenet large scale visual recognition challenge. *IJCV*, 2015.
- [43] Tsung-Yi Lin, Michael Maire, Serge Belongie, James Hays, Pietro Perona, Deva Ramanan, Piotr Dollár, and C Lawrence Zitnick. Microsoft coco: Common objects in context. In *ECCV*, 2014.
- [44] Ning Xu, Linjie Yang, Yuchen Fan, Dingcheng Yue, Yuchen Liang, Jianchao Yang, and Thomas Huang. Youtube-vos: A large-scale video object segmentation benchmark. *arXiv*, 2018.
- [45] Volodymyr Mnih and Geoffrey Hinton. Learning to label aerial images from noisy data. In *ICML*, 2012.
- [46] Honglie Chen, Weidi Xie, Andrea Vedaldi, and Andrew Zisserman. Autocorrect: Deep inductive alignment of noisy geometric annotations. In *BMVC*, 2019.

- [47] Olaf Ronneberger, Philipp Fischer, and Thomas Brox. U-net: Convolutional networks for biomedical image segmentation. In *MICCAI*, 2015.
- [48] Kaiming He, Xiangyu Zhang, Shaoqing Ren, and Jian Sun. Deep residual learning for image recognition. In *CVPR*, 2016.
- [49] Linjie Yang, Yanran Wang, Xuehan Xiong, Jianchao Yang, and Aggelos K Katsaggelos. Efficient video object segmentation via network modulation. In *CVPR*, 2018.
- [50] Federico Perazzi, Anna Khoreva, Rodrigo Benenson, Bernt Schiele, and Alexander Sorkine-Hornung. Learning video object segmentation from static images. In *CVPR*, 2017.
- [51] Seoung Wug Oh, Joon-Young Lee, Kalyan Sunkavalli, and Seon Joo Kim. Fast video object segmentation by reference-guided mask propagation. In *CVPR*, 2018.
- [52] Joakim Johnander, Martin Danelljan, Emil Brissman, Fahad Shahbaz Khan, and Michael Felsberg. A generative appearance model for end-to-end video object segmentation. In *CVPR*, 2019.

Appendix

A Architecture details

We present a more detailed description of our encoder networks illustrated in Figure 5. Specifically, we adopt a ResNet-18 with the channel number and stride number of the residual blocks reduced in our case. For the appearance model, we take a standard U-Net [47] structure with ResNet-18 as the backbone encoder.

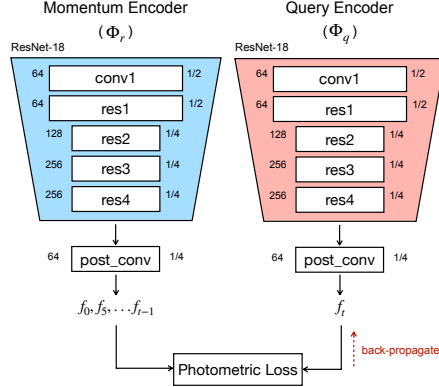


Figure 5: The structure of the momentum memory encoders. Two trapezoids refer two ResNet-18 based encoders, in which each rectangle denotes either a convolution layer or a residual block. The number on the left of the rectangle shows the out channel number of that layer, e.g. 64, 128, 256, while the number on the right shows the resolution ratio of the output feature map, e.g. 1/2.

B More training details

Occlusion-aware mask propagation. While training, we use the same restricted attention mechanism as in [7], to compute the similarity between paired frames. That is, each pixel in the current frame is only reconstructed by the pixels within a local window in the reference frames. In practice, we apply a 25×25 window to perform matching on 96×96 feature maps. Empirically, larger window size is beneficial for more accurate matching to a certain extent, due to the expense of more perturbation in a larger window.

Online adaptation. For each individual video sequence, we leverage an appearance model to perform online adaptation. To segment a certain video frame, the appearance model is trained with all the frames that have been predicted from the correspondence propagation. The numbers of segmented objects in different video sequences are not the same, where we need to specify the output channel number of the appearance model for each video based on its first annotation frame. During training, we use both the pixel-wise cross entropy loss and the Dice loss to optimize the model. Under the assumption that former propagated masks contain less error accumulation and have better quality, we put more weights on the early frames in the video sequence, since they are less prone to drift. Details can be checked in the code.

C More results

In this section, we provide more qualitative results on DAVIS-2017 and YouTube-VOS dataset.

C.1 More qualitative results.

Various difficult cases are shown in Figure 6 and 7. From the visualisation results, objects motion, large camera motion, cases where multiple objects co-exist, and pose variations can all be well solved by our proposed model.

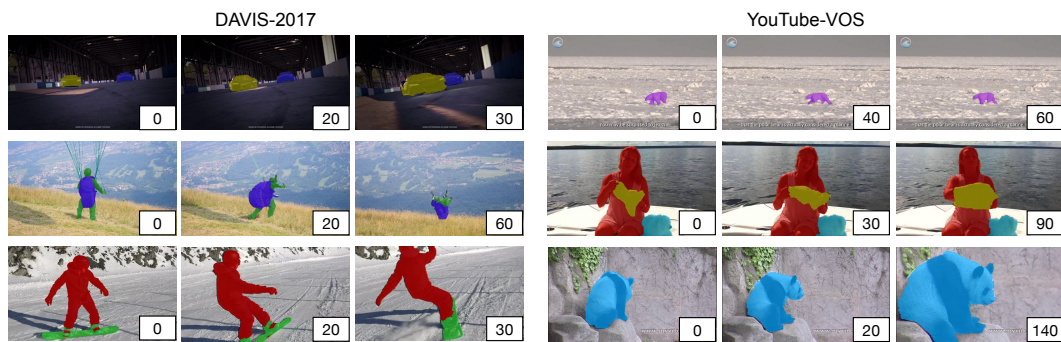


Figure 6: More qualitative results on DAVIS-2017 and YouTube-VOS datasets. The first row shows the scale change and gradual occlusion case. The second row shows the appearance and pose variation of the tracking object. The third row shows significant camera shaking and object motion. YouTube-VOS: The first row shows the motion of the white polar bear, whose color is so similar with the background ice that makes it difficult for accurate tracking. The second row shows the process of the person putting on her elbow guard with occlusion and dis-occlusion involved. The third row shows the motion and scale change of the panda.

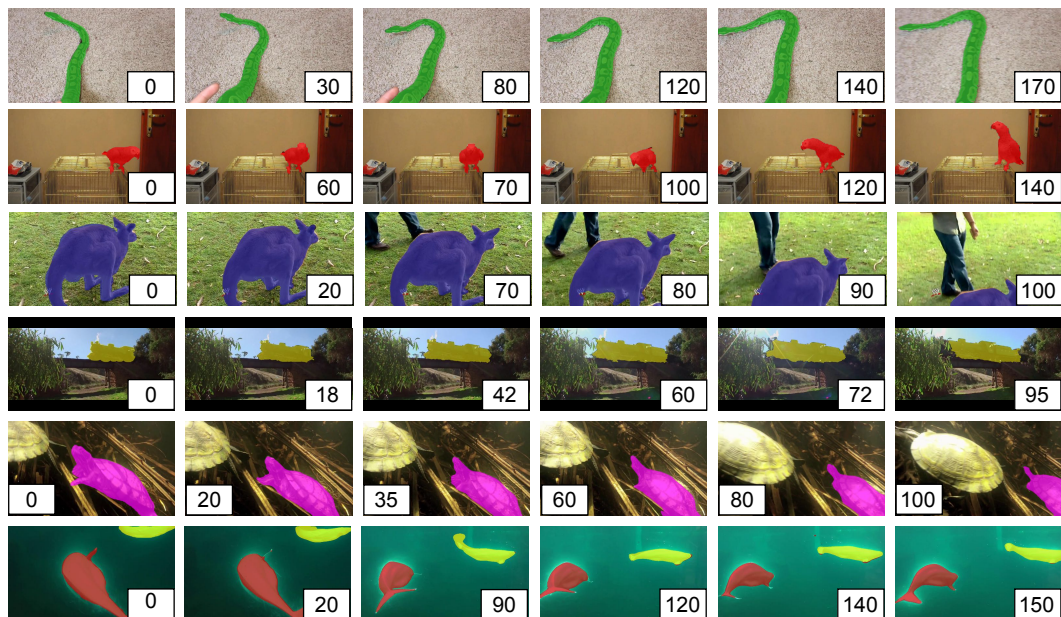


Figure 7: More qualitative results on YouTube-VOS dataset. The first two rows show moving objects and pose variations among objects. Row 3-5 show occlusion and dis-occlusion (out of the scene) scenarios. The sixth row shows tracking under multiple moving objects.

C.2 More qualitative comparison.

We show predictions from each separate proposed module in Figure 8 and 9. In Figure 8, both the pose of the bird and the piglet vary a lot in the video. In addition, there is great appearance change in the bird object, yet our model is still able to produce good segmentation masks. As shown in the visualisation results, the pairwise model tends to drift when the object has sharp pose variation or abrupt camera shaking between the paired frames. By adding the momentum memory, the model will compensate for the occlusion / dis-occlusion area in the previous frame by leveraging information from other previous frames, but the model is still prone to drift due to the fact that the intensities or colors of the foreground and background are highly similar. As shown in Figure 9, online adaptation helps tackling this problem and clearing up some background drifts, as well as making segmentation masks smoother.

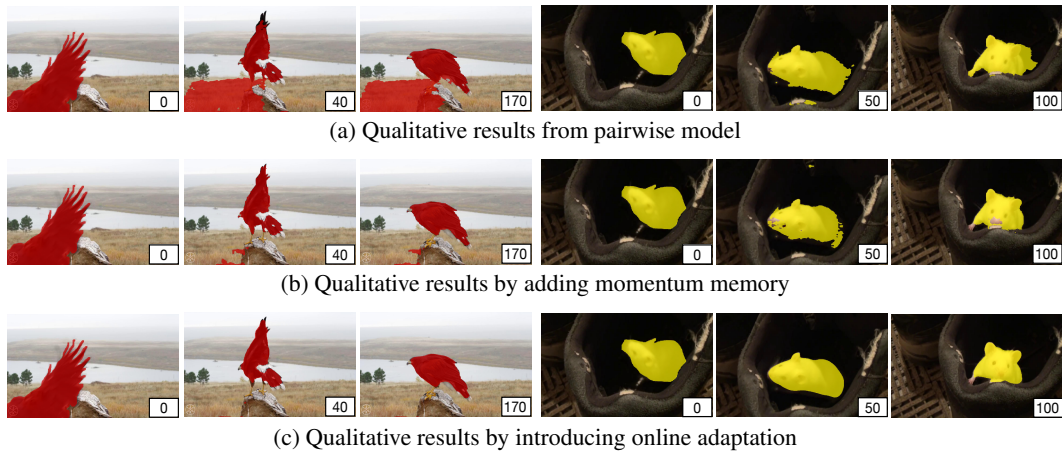


Figure 8: Qualitative comparison on YouTube-VOS dataset for the effectiveness of the proposed modules.

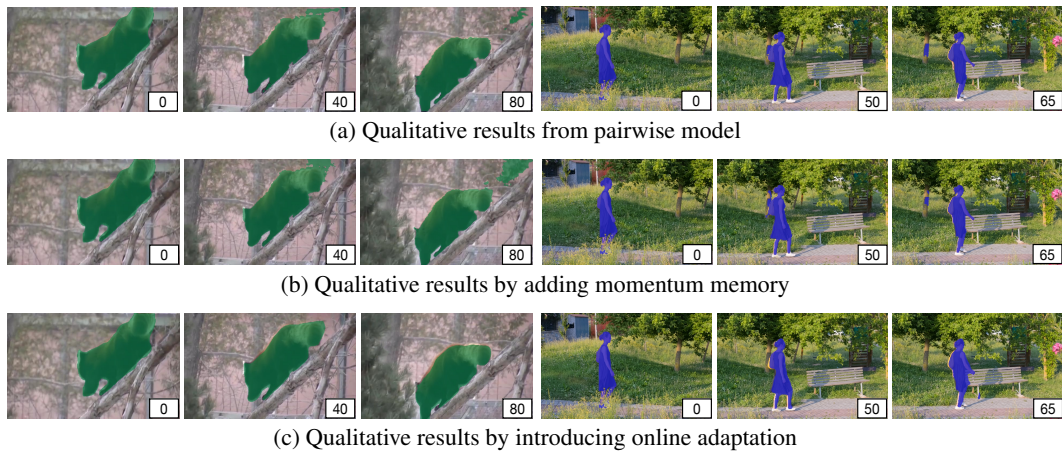


Figure 9: Qualitative comparisons on YouTube-VOS dataset (left) and DAVIS-2017 train set (right) for the effectiveness of the proposed modules.

C.3 Visualisation of the online adaptation process.

We show the adapted results from the appearance model of different training iterations in Figure 10 and 11. The propagated masks used for training the appearance model contain drifts in the background. The figure indicates that during training, the appearance model first learns the self-similarity among object masks before fitting to the error drifts.

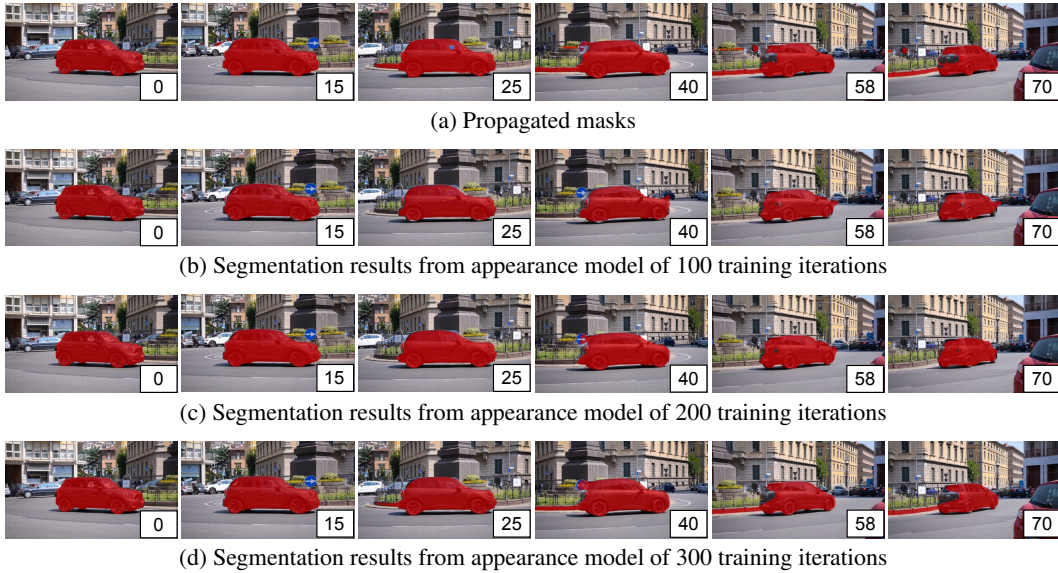


Figure 10: The visualisation results (DAVIS-2017) from the appearance model of different training iterations.

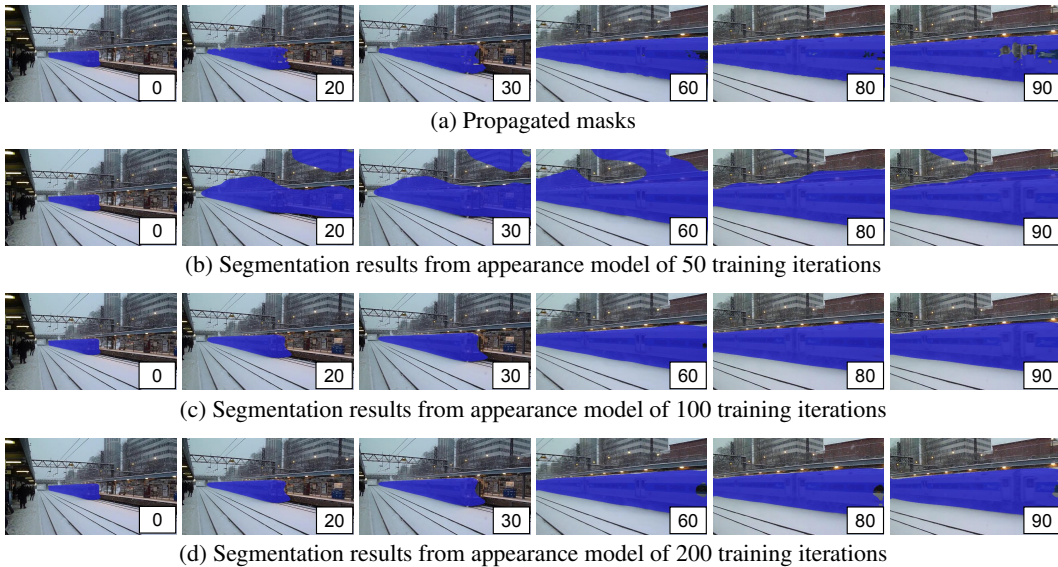


Figure 11: The visualisation results (YouTube-VOS) from the appearance model of different training iterations.